

Bounds on Heavy-to-Heavy Mesonic Form Factors

Cheng-Wei Chiang* and Adam K. Leibovich†

Department of Physics, Carnegie Mellon University, Pittsburgh, PA 15213

Abstract

We provide upper and lower bounds on the form factors for $B \rightarrow D, D^*$ by utilizing inclusive heavy quark effective theory sum rules. These bounds are calculated to leading order in Λ_{QCD}/m_Q and α_s . The $O(\alpha_s^2 \beta_0)$ corrections to the bounds at zero recoil are also presented. We compare our bounds with some of the form factor models used in the literature. All the models we investigated failed to fall within the bounds for the combination of form factors $(\omega^2 - 1)/(4\omega)|\omega h_{A2} + h_{A3}|^2$.

*chengwei@andrew.cmu.edu

†adaml@cmuhep2.phys.cmu.edu

I. INTRODUCTION

Currently, heavy-to-heavy form factors are mainly derived from models. Since models are used in Monte Carlos, which in turn feeds into studies of backgrounds and efficiencies in many experimental settings, constraining them is very important. Model independent information on the form factors can be obtained from the Heavy Quark Effective Theory (HQET). HQET [1–3] vastly simplifies the nonperturbative calculation of form factors by relating all of them in the infinite mass limit to a single universal Isgur-Wise function, ξ , which describes the nonperturbative physics of the light degrees of freedom in the heavy mesons. This function is normalized to unity at zero recoil, where the heavy meson in the final state has the same velocity as the initial one. Nonetheless, HQET does not predict the explicit form of the Isgur-Wise function.

Since it is not possible to calculate heavy-to-heavy form factors from first principles, the next best thing to do is to theoretically bound them.¹ A set of model independent bounds on form factors have been derived [5,6], and can serve as a consistency condition for phenomenological models. Bounds to $\mathcal{O}(1/m_Q)$ at arbitrary momentum transfer had been presented in [6,7] for heavy-to-heavy and heavy-to-light form factors. However, as noted in [6–8], the lower bound is sensitive to the perturbative corrections, and leading order in α_s correction should be included to provide more reliable bounds. Therefore, in this work we present an analysis of the leading QCD corrections on the bounds of individual heavy-to-heavy, more specifically $B \rightarrow D^{(*)}\ell\bar{\nu}$, form factors. The information of these bounds will help us rule out unrealistic models, and may in turn be applied to certain decay amplitudes that are of interest.

This paper is organized as follows. In Section II, we review the derivation of the sum rules used to obtain the model-independent bounds on form factors defined in Section III. Section III also gives the proper combinations of structure functions used later for the

¹See, however, [4] for model independent parameterizations of the form factors.

bounds on each of the form factors. In Section IV, we perform the tree level nonperturbative expansion and first order QCD perturbative calculation to eliminate the leading uncertainty in the bounds. Section V provides the bounds on individual form factors explicitly with the structure functions given in the Appendix, and discusses various influences of the parameters appearing in the expansion of the bounds. Some popular form factor models are compared with our bounds in Section VI. Order $\alpha_S^2 \beta_0$ corrections to the bounds at zero recoil are computed in Section VII. The conclusion of our work is summarized in Section VIII. The Appendix lists the perturbative corrections to the structure functions.

II. REVIEW OF SUM RULES

The sum rules are derived by relating the inclusive decay rate, calculated using the operator product expansion (OPE) and perturbative QCD, to the sum of exclusive decay rates. In the following, we follow [6,8] in the derivation of the bounds.

First, consider the time ordered product of two currents between B mesons in the momentum space,

$$\begin{aligned} T^{\mu\nu} &= \frac{i}{2M_B} \int d^4x e^{-iq\cdot x} \langle B(v) | T(J^{\mu\dagger}(x) J^\nu(0)) | B(v) \rangle \\ &= -g^{\mu\nu} T_1 + v^\mu v^\nu T_2 + i\epsilon^{\mu\nu\alpha\beta} q_\alpha v_\beta T_3 + q^\mu q^\nu T_4 + (q^\mu v^\nu + v^\mu q^\nu) T_5, \end{aligned} \quad (1)$$

where J^μ is a $b \rightarrow c$ axial or vector current. The time ordered product can be expressed as a sum over hadronic or partonic intermediate states. The sum over hadronic states includes the matrix element $\langle H | J | B \rangle$, where $H = D, D^{(*)}$ is the final state heavy meson of interest. After inserting a complete set of states and dotting with four vectors $a_\mu^* a_\nu$, one obtains

$$\begin{aligned} T(\epsilon) &= \frac{1}{2M_B} \sum_X (2\pi)^3 \delta^3(\vec{p}_X + \vec{q}) \frac{|\langle X | a \cdot J | B \rangle|^2}{E_X - E_H - \epsilon} \\ &\quad + \frac{1}{2M_B} \sum_X (2\pi)^3 \delta^3(\vec{p}_X - \vec{q}) \frac{|\langle B | a \cdot J | X \rangle|^2}{\epsilon + E_X + E_H - 2M_B}, \end{aligned} \quad (2)$$

where $T(\epsilon) \equiv a_\mu^* T^{\mu\nu} a_\nu$, $\epsilon = M_B - E_H - v \cdot q$, and the sum over X includes the usual $d^3p/2E_X$ for each particle in the state X . We choose to work in the rest frame of the B

meson, $p = M_B v$, and the z axis pointing in the direction of \vec{q} . We will hold q_3 fixed while analytically continuing $v \cdot q$ to the complex plane. $E_H = \sqrt{M_H^2 + q_3^2}$ is the H meson energy. There are two cuts in the complex ϵ plane, $0 < \epsilon < \infty$, corresponding to the decay process $b \rightarrow c$, and $-\infty < \epsilon < -2E_H$, corresponding to two b quarks and a \bar{c} quark in the final state. The second cut will not be important for our discussion.

The integral over ϵ of the time ordered product, $T(\epsilon)$, times a weight function, $\epsilon^n W_\Delta(\epsilon)$ can be computed perturbatively in QCD [6,8]. For simplicity, we pick the weight function $W_\Delta(\epsilon) = \theta(\Delta - \epsilon)$, which corresponds to summing over all hadronic resonances up to the excitation energy Δ with equal weight. Relating the integral with the hard cutoff to the exclusive states requires local duality at the scale Δ . Δ must be chosen large enough so that the structure functions can be calculated perturbatively.

Taking the zeroth moment of $T(\epsilon)$

$$\begin{aligned} \frac{1}{2\pi i} \int_C d\epsilon \theta(\Delta - \epsilon) T(\epsilon) &= \sum_X \theta(E_X - E_M - \Delta) (2\pi)^3 \delta^3(\vec{q} + \vec{p}_X) \frac{|\langle X | J \cdot a | B \rangle|^2}{2M_B} \\ &\geq \frac{|\langle H(v') | a \cdot J | B(v) \rangle|^2}{4M_B E_H} \end{aligned} \quad (3)$$

gives an upper bound on the matrix element.

The first moment of $T(\epsilon)$ gives

$$\begin{aligned} \frac{1}{2\pi i} \int_C d\epsilon \epsilon \theta(\Delta - \epsilon) T(\epsilon) &= \sum_{X \neq H} \theta(\Delta - E_X + E_H) (E_X - E_H) (2\pi)^3 \delta^3(p_X + q) \frac{|\langle X | a \cdot J | B \rangle|^2}{4M_B E_X} \\ &\geq (E_1 - E_H) \sum_{X \neq H} \theta(\Delta - E_X + E_H) (2\pi)^3 \delta^3(p_X + q) \frac{|\langle X | a \cdot J | B \rangle|^2}{4M_B E_X}. \end{aligned} \quad (4)$$

where E_1 denotes the first excited state that is more massive than H meson. Here the validity of the inequality relies on the assumption that multiparticle final states with less energy than E_1 contribute negligibly. This assumption is true in large N_c , and is also confirmed by current experimental data.

A lower bound can be formed by combining Eqs. (3) and (4) to be

$$\frac{|\langle H(v') | a \cdot J | B(v) \rangle|^2}{4M_B E_H} \geq \frac{1}{2\pi i} \int_C d\epsilon \theta(\Delta - \epsilon) T(\epsilon) \left(1 - \frac{\epsilon}{E_1 - E_H}\right). \quad (5)$$

Therefore, we find the bounds

$$\begin{aligned} \frac{1}{2\pi i} \int_C d\epsilon \theta(\Delta - \epsilon) T(\epsilon) \left(1 - \frac{\epsilon}{E_1 - E_H}\right) &\leq \frac{|\langle H(v') | a \cdot J | B(v) \rangle|^2}{4M_B E_H} \\ &\leq \frac{1}{2\pi i} \int_C d\epsilon \theta(\Delta - \epsilon) T(\epsilon). \end{aligned} \quad (6)$$

As emphasized in [8], the upper bound is essentially model independent while the lower bound relies on the assumption about the final state spectrum. These bounds can be used for the decays at arbitrary momentum transfer q^2 and are good for both heavy mesons and baryons. (For baryons, a spin sum $\frac{m_H}{2J+1} \sum_{S,S'}$ needs to be included in front of the bounded factor.)

Since $1/(E_1 - E_H) \sim 1/\Lambda_{\text{QCD}}$, the lower bounds will be limited to order in $1/m_Q$. The upper bounds, on the other hand, can be calculated to order $1/m_Q^2$ without additional HQET parameters.

III. HADRONIC SIDE

The hadronic matrix elements for semi-leptonic decay of a B meson into a pseudoscalar meson P or a vector meson V may be parameterized as

$$\begin{aligned} \frac{\langle P(v') | V^\mu | B(v) \rangle}{\sqrt{M_P M_B}} &= h_+(\omega) (v + v')^\mu + h_-(\omega) (v - v')^\mu, \\ \frac{\langle V(v', \varepsilon) | V^\mu | B(p) \rangle}{\sqrt{M_V M_B}} &= i h_V(\omega) \epsilon^{\mu\nu\alpha\beta} \varepsilon_\nu^* v'_\alpha v_\beta, \\ \frac{\langle V(v', \varepsilon) | A^\mu | B(v) \rangle}{\sqrt{M_V M_B}} &= h_{A_1}(\omega) (\omega + 1) \varepsilon^{*\mu} - [h_{A_2}(\omega) v^\mu + h_{A_3}(\omega) v'^\mu] v \cdot \varepsilon^*. \end{aligned} \quad (7)$$

v' is the velocity of the final state meson, and the variable $\omega = v \cdot v'$ is a measure of the recoil. One may relate ω to the momentum transfer q^2 by $\omega = (M_B^2 + M_H^2 - q^2)/(2M_B M_H)$. Therefore, with a proper choices of the current J^μ and the four vector a^μ , one may readily select the form factor of interest and the corresponding sum rule for bounding. In the heavy quark symmetry limit, these form factors satisfy relations [1,2]

$$\begin{aligned}
h_+(\omega) &= h_V(\omega) = h_{A_1}(\omega) = h_{A_3}(\omega) = \xi(\omega), \\
h_+(\omega) &= h_{A_1}(\omega) = 0.
\end{aligned} \tag{8}$$

To bound h_{A_1} (or h_V), one may choose $J^\mu = A^\mu$ (or V^μ) and $a^\mu = (0, 1, 0, 0)$. Then the factor to be bounded is $\frac{(\omega+1)^2}{4\omega} |h_{A_1}(\omega)|^2 \left(\frac{\omega^2-1}{4\omega} |h_V(\omega)|^2 \right)$ and the sum rule used to bound is $T_{1OPE} = T_{1Hadronic}$. The corresponding first excited state more massive than D^* that contributes to the sum rule is the $J^P = 1^+$ state, *i.e.* D_1 , since scalars do not contribute to T_1 .

For h_+ , one may take $J^\mu = V^\mu$ and $a^\mu = (1 + E_D/M_D, 0, 0, -q_3/M_D)$. Then the factor to be bounded is $\frac{(\omega+1)^2}{\omega} |h_+(\omega)|^2$, and the combination of structure functions used in bounds is

$$\begin{aligned}
T(\epsilon) &= -2(1 + \omega) T_1 + (1 + \omega)^2 T_2 + (M_B - M_D - \epsilon)^2 (1 + \omega)^2 T_4 \\
&\quad + 2(M_B - M_D - \epsilon) (1 + \omega)^2 T_5.
\end{aligned} \tag{9}$$

Since $a^\mu = v^\mu + v'^\mu$, the first excited resonance that can contribute in this case is D_1 , due to the $\epsilon^{\mu\nu\alpha\beta}$ structure of the D^* form factor.

Similarly, a convenient choice to isolate h_- is to choose $J^\mu = V^\mu$ and $a^\mu = (1 - E_D/M_D, 0, 0, q_3/M_D)$. Thus,

$$\begin{aligned}
T(\epsilon) &= -2(1 - \omega) T_1 + (1 - \omega)^2 T_2 + (M_B + M_D - \epsilon)^2 (1 - \omega)^2 T_4 \\
&\quad + 2(M_B + M_D - \epsilon) (1 - \omega)^2 T_5
\end{aligned} \tag{10}$$

bounds $\frac{(\omega-1)^2}{\omega} |h_-(\omega)|^2$. D_1 would be the first excited resonance for the same reason as in the case of h_+ .

It is impossible to single out h_{A_2} and h_{A_3} individually by any choice of a^μ . One good choice is to take $J^\mu = A^\mu$ and $a^\mu = (E_D/M_D, 0, 0, -q_3/M_D)$. Then

$$\begin{aligned}
T(\epsilon) &= -T_1 + \omega^2 T_2 + (M_B \omega - M_D^* - \epsilon)^2 T_4 \\
&\quad + 2\omega (M_B \omega - M_D^* - \epsilon) T_5
\end{aligned} \tag{11}$$

is the combination for bounding $\frac{\omega^2-1}{4\omega} |\omega h_{A_2}(\omega) + h_{A_3}(\omega)|^2$. The first excited resonance that would contribute in this case would be the unobserved D_0^* .

IV. PARTONIC SIDE

Due to the heavy quark masses appearing in the problem, both the strong coupling constant $\alpha_s(m_Q)$ (~ 0.3 at 2 GeV) and Λ_{QCD}/m_Q will be good expansion parameters. Since ω is never very far from one, expanding in $\omega - 1$ is also possible. We will keep terms up to order $\alpha_s(w - 1)$, dropping terms of order $\alpha_s(w - 1)^2$, α_s^2 , $\Lambda_{\text{QCD}}^2/m_Q^2$ and $\alpha_s \Lambda_{\text{QCD}}/m_Q$.

The structure functions can be decomposed as

$$T_i^{full} = T_i^{1/m} + T_i^{\alpha_s}, \quad (12)$$

where the term $T_i^{1/m}$ contains the tree and Λ_{QCD}/m_Q contribution to the structure function, which has previously been calculated [9–11]. For these nonperturbative corrections, we keep the full ω dependence.

The leading order α_s corrections consist of bremsstrahlung radiation of a gluon from the heavy quarks and one loop virtual corrections. We expand to first order in $w - 1$, defining

$$T_i^{\alpha_s} = \frac{\alpha_s}{\pi} [U_i + (w - 1) V_i]. \quad (13)$$

The final results for the functions U_i and V_i are presented in the Appendix. The perturbative corrections to T_1 were previously calculated in [12,8], and agree with the results found here.

We define the moments of the structure functions as

$$\frac{1}{2\pi i} \int d\epsilon \epsilon^n T_i = I_i^{(n)} + A_i^{(n)}, \quad (14)$$

where

$$\begin{aligned} I_i^{(n)} &= \frac{1}{2\pi i} \int d\epsilon \epsilon^n T_i^{1/m}, \\ A_i^{(n)} &= \frac{1}{2\pi i} \int d\epsilon \epsilon^n \frac{\alpha_s}{\pi} [U_i + (w - 1) V_i]. \end{aligned} \quad (15)$$

The moments of $T_i^{1/m}$ can be found in [5,6]. The moments for the perturbative corrections can be straightforwardly obtained from the functions in the Appendix. One thing to be noted is that the integration variable ϵ in the bounds was defined in terms of hadronic variables. So

when relating to the partonic computations, the corresponding integration variable should be changed to the one defined by partonic variables, namely, $\epsilon_p = m_b - m_c - v \cdot q$. The relation between them is $\epsilon_h = \epsilon_p + \delta$, with $\delta = E_c - E_H + M_B - m_b$ and E_c being the energy of the c-quark. We can now use these definitions to calculate the bounds on the form factors.

V. BOUNDS ON INDIVIDUAL FORM FACTORS

To form the bounds, one just takes the proper moments of the structure functions to form the combination required in the sum rules given in Section III. Corrections of order $\Lambda_{\text{QCD}}^2/m_Q^2$, α_s^2 , $\alpha_s \Lambda_{\text{QCD}}/m_Q$, and $\alpha_s (\omega - 1)^2$ should be small and have been neglected. To this order, the Λ_{QCD}/m_Q corrections will depend on 3 HQET parameters; $\bar{\Lambda}$, λ_1 and λ_2 . From the measured mass difference, $M_{D^*} - M_D$, a very accurate value of λ_2 can be determined, $\lambda_2 = 0.12 \text{ GeV}^2$. It is very difficult to measure the parameters $\bar{\Lambda}$ and λ_1 individually, but a certain linear combination is much better determined [13]. We will use three different parameter sets to show the dependence on $\bar{\Lambda}$ and λ_1 : (A) $\bar{\Lambda} = 0.4 \text{ GeV}$ and $\lambda_1 = -0.2 \text{ GeV}^2$, (B) $\bar{\Lambda} = 0.3 \text{ GeV}$ and $\lambda_1 = -0.1 \text{ GeV}^2$, (C) $\bar{\Lambda} = 0.5 \text{ GeV}$ and $\lambda_1 = -0.3 \text{ GeV}^2$.

The sum rule for bounding $(\omega + 1)^2 |h_{A_1}(\omega)|^2 / (4\omega)$ uses T_1 with the axial-axial current. The upper bound is simply the zeroth moment of T_1 , which is by Eq. (6)

$$\frac{(\omega + 1)^2}{4\omega} |h_{A_1}(\omega)|^2 \leq I_1^{(0)AA} + A_1^{(0)AA}. \quad (16)$$

The variable λ used for regularizing infrared divergences in the kinematic region away from zero recoil disappears in the final result. The first moment of T_1 is needed for the lower bound, which is

$$\frac{(\omega + 1)^2}{4\omega} |h_{A_1}(\omega)|^2 \geq I_1^{(0)AA} + A_1^{(0)AA} - \frac{1}{E_{D_1} - E_{D^*}} (I_1^{(1)AA} + A_1^{(1)AA}) \quad (17)$$

The upper and lower bounds are shown in Fig. 1.² For this section, the dotted curves are

²For all the figures in this section we take $m_b = 4.8 \text{ GeV}$, $m_c = 1.4 \text{ GeV}$, $\alpha_s = 0.3$ (corresponding to a scale of about 2 GeV), and $\lambda_2 = 0.12 \text{ GeV}^2$. The values of $\bar{\Lambda}$ and λ_1 are discussed in the text.

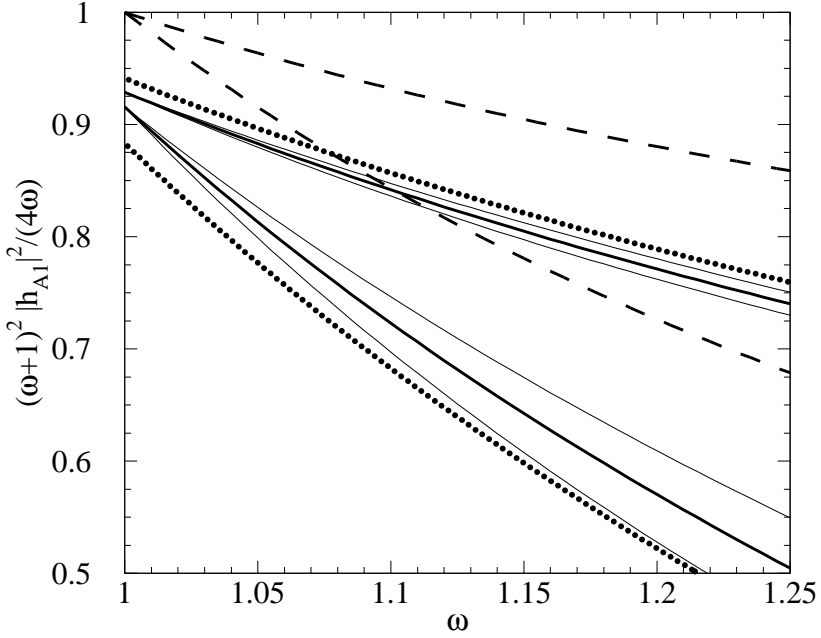


FIG. 1. *Upper and lower bounds on $(\omega + 1)^2 |h_{A1}(\omega)|^2 / (4\omega)$. The thick solid (dotted) curves are the upper and lower bounds including perturbative corrections for HQET parameter set (A) described in the text, and $\Delta = 1$ GeV (2 GeV). The dashed curves are the bounds without perturbative corrections, also for HQET parameter set (A). The thin solid curves show the dependence on $\bar{\Lambda}$ and λ_1 , using parameter sets (B) and (C), with $\Delta = 1$ GeV.*

the bounds without perturbative corrections using set (A) above, while the solid and dashed curves represent the bounds including the perturbative corrections with $\Delta = 1$ GeV and $\Delta = 2$ GeV, respectively. We have shown the bounds in the kinematic range $1 \leq \omega \lesssim 1.25$, where the higher order correction $\alpha_s(\omega - 1)^2$ should be negligible. The thin solid curves use the other HQET parameter sets (B) and (C).

A similar set of bounds for $(\omega^2 - 1) |h_V(\omega)|^2 / (4\omega)$ can be obtained readily by changing AA (axial-axial currents) to VV (vector-vector currents) in the above formulae. The bounds in this case are shown in Fig. 2. The tree level bounds go to zero at zero recoil because of the $\omega - 1$ factor.

The bounds on the other form factors involve higher moments of T_4 and T_5 . The upper bound for $(\omega + 1)^2 |h_+(\omega)|^2 / \omega \leq h_+^{upper}$, where

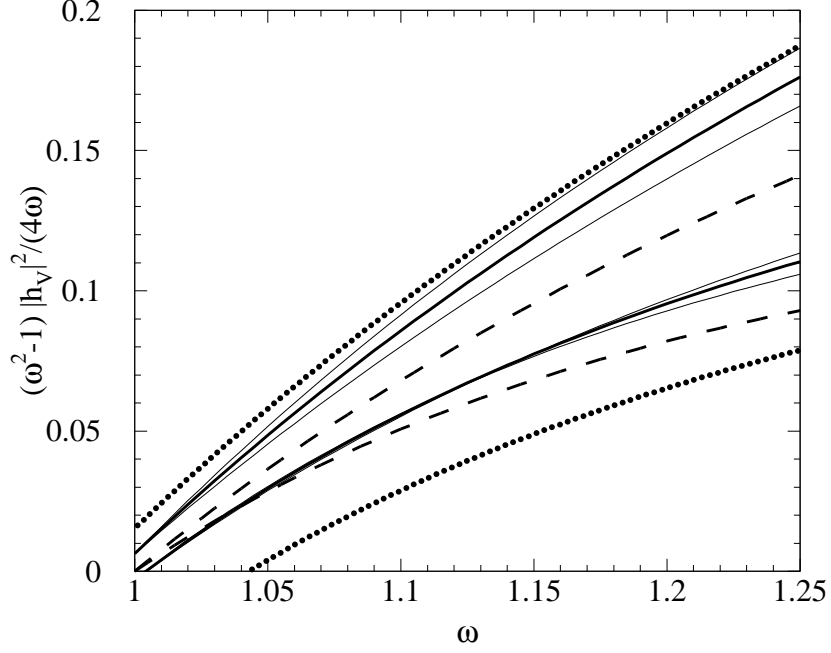


FIG. 2. *Upper and lower bounds on $(\omega^2 - 1) |h_V(\omega)|^2 / (4\omega)$. The thick solid (dotted) curves are the bounds with perturbative corrections for HQET parameter set (A), and $\Delta = 1$ GeV (2 GeV). The dashed curves are the bounds without perturbative corrections, also for HQET parameter set (A). The thin solid curves show the dependence on $\bar{\Lambda}$ and λ_1 , using parameter sets (B) and (C), with $\Delta = 1$ GeV.*

$$h_+^{upper} = (1 + \omega)^2 \left\{ -2 \frac{1}{1 + \omega} I_1^{(0)VV} + I_2^{(0)VV} + I_4^{(2)VV} - 2(M_B - M_D) I_4^{(1)VV} \right. \\ \left. + (M_B - M_D)^2 I_4^{(0)VV} + 2(M_B - M_D) I_5^{(0)VV} - 2I_5^{(1)VV} \right. \\ \left. - 2 \frac{1}{1 + \omega} A_1^{(0)VV} + A_2^{(0)VV} + A_4^{(2)VV} - 2(M_B - M_D) A_4^{(1)VV} \right. \\ \left. + (M_B - M_D)^2 A_4^{(0)VV} + 2(M_B - M_D) A_5^{(0)VV} - 2A_5^{(1)VV} \right\}. \quad (18)$$

The lower bound is $(\omega + 1)^2 |h_+(\omega)|^2 / \omega \geq h_+^{lower}$, where

$$h_+^{lower} = h_+^{upper} \\ - \frac{(1 + \omega)^2}{M_{D_1} - M_D} \left\{ -2 \frac{1}{1 + \omega} I_1^{(1)VV} + I_2^{(1)VV} + I_4^{(3)VV} - 2(M_B - M_D) I_4^{(2)VV} \right. \\ \left. + (M_B - M_D)^2 I_4^{(1)VV} + 2(M_B - M_D) I_5^{(1)VV} - 2I_5^{(2)VV} \right. \\ \left. - 2 \frac{1}{1 + \omega} A_1^{(1)VV} + A_2^{(1)VV} + A_4^{(3)VV} - 2(M_B - M_D) A_4^{(2)VV} \right\} \quad (19)$$

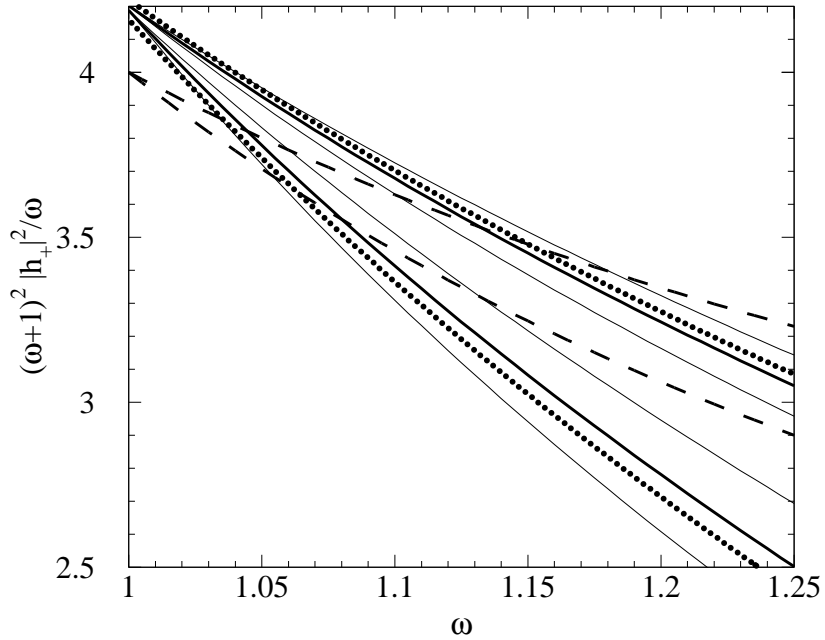


FIG. 3. *Upper and lower bounds on $(\omega+1)^2 |h_+(\omega)|^2 / \omega$. The thick solid (dotted) curves are the bounds with perturbative corrections for HQET parameter set (A), and $\Delta = 1$ GeV (2 GeV). The dashed curves are the bounds without perturbative corrections, also for HQET parameter set (A). The thin solid curves show the dependence on $\bar{\Lambda}$ and λ_1 , using parameter sets (B) and (C), with $\Delta = 1$ GeV.*

$$+ (M_B - M_D)^2 A_4^{(1)VV} + 2(M_B - M_D) A_5^{(1)VV} - 2A_5^{(2)VV} \} .$$

They are plotted in Fig. 3. The perturbative physics pushes the bounds up from the tree level bounds in the region near the maximal momentum transfer while drags them down at large recoil. Changing Δ from 1 GeV to 2 GeV only slightly loosens both bounds.

Without explicitly writing out the bounds on $(\omega - 1)^2 |h_-(\omega)|^2 / \omega$, we simply state that they can be obtained from Eq. (18) and (19) by: 1) replacing each $(1 + \omega)$ factor by $(1 - \omega)$ and 2) substituting $M_B - M_D$ by $M_B + M_D$. The bounds on this form factor are shown in Fig. 4. Notice that in this case, both the upper and lower bounds at tree level are identically zero. The perturbative corrections push both bounds away from zero. We still plot these negative lower bounding curves for reference even though the real lower bounds should be

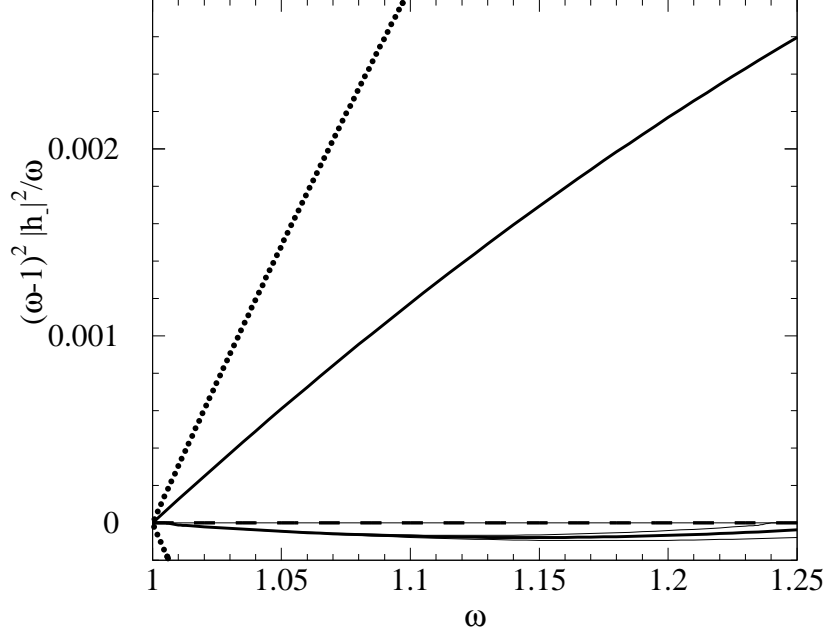


FIG. 4. *Upper and lower bounds on $(\omega-1)^2|h_-(\omega)|^2/\omega$. The thick solid (dotted) curves are the bounds with perturbative corrections for HQET parameter set (A), and $\Delta = 1$ GeV (2 GeV). The dashed curves are the bounds without perturbative corrections, also for HQET parameter set (A). The thin solid curves show the dependence on $\bar{\Lambda}$ and λ_1 , using parameter sets (B) and (C), with $\Delta = 1$ GeV.*

zero since the factors we are bounding are all positive-definite. Using $\Delta = 2$ GeV in the calculation widens the upper bound by more than a factor of 2.

Similarly, the upper bound for $(\omega^2 - 1) |\omega h_{A_2}(\omega) + h_{A_3}(\omega)|^2 / (4\omega) \leq h_{A_3}^{upper}$, where

$$\begin{aligned}
h_{A_3}^{upper} = & -I_1^{(0)AA} + \omega^2 I_2^{(0)AA} + (M_B\omega - M_{D^*})^2 I_4^{(0)AA} - 2\omega(M_B\omega - M_{D^*}) I_4^{(1)AA} \\
& + \omega^2 I_4^{(2)AA} + 2\omega(M_B\omega - M_{D^*}) I_5^{(0)AA} - 2\omega^2 I_5^{(1)AA} \\
& - A_1^{(0)AA} + \omega^2 A_2^{(0)AA} + (M_B\omega - M_{D^*})^2 A_4^{(0)AA} - 2\omega(M_B\omega - M_{D^*}) A_4^{(1)AA} \\
& + \omega^2 A_4^{(2)AA} + 2\omega(M_B\omega - M_{D^*}) A_5^{(0)AA} - 2\omega^2 A_5^{(1)AA},
\end{aligned} \tag{20}$$

while the lower bound $(\omega^2 - 1) |\omega h_{A_2}(\omega) + h_{A_3}(\omega)|^2 / (4\omega) \leq h_{A_3}^{lower}$, where

$$h_{A_3}^{lower} = h_{A_3}^{upper} - \frac{1}{M_{D_1} - M_{D^*}} \left\{ -I_1^{(1)AA} + \omega^2 I_2^{(1)AA} + (M_B\omega - M_{D^*})^2 I_4^{(1)AA} \right. \tag{21}$$

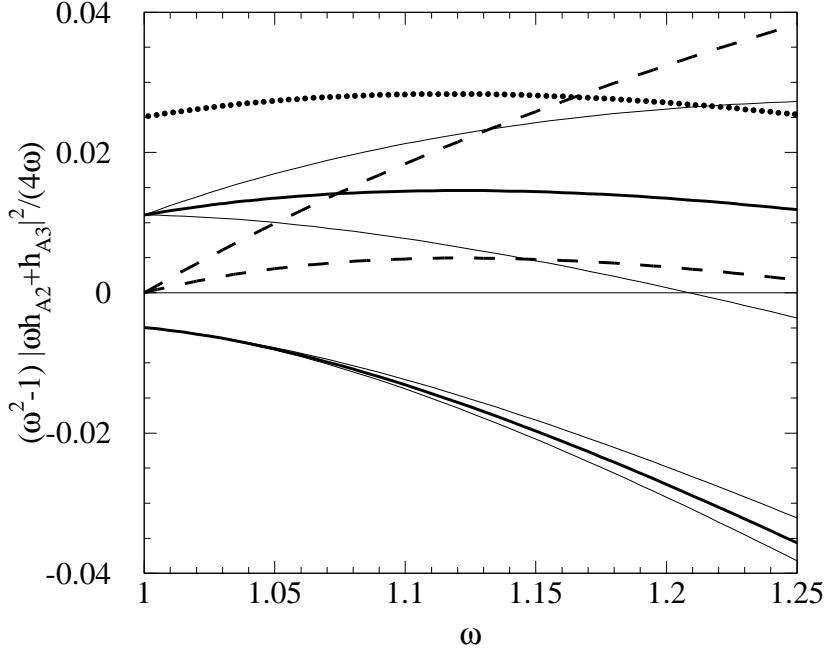


FIG. 5. *Upper and lower bounds on $(\omega^2 - 1) |wh_{A2}(\omega) + h_{A3}(\omega)|^2 / (4\omega)$. The thick solid (dotted) curves are the bounds with perturbative corrections for HQET parameter set (A), and $\Delta = 1$ GeV (2 GeV). The dashed curves are the bounds without perturbative corrections, also for HQET parameter set (A). The thin solid curves show the dependence on $\bar{\Lambda}$ and λ_1 , using parameter sets (B) and (C), with $\Delta = 1$ GeV.*

$$\begin{aligned}
& -2\omega(M_B\omega - M_{D^*})I_4^{(2)AA} + \omega^2 I_4^{(3)AA} + 2\omega(M_B\omega - M_{D^*})I_5^{(1)AA} - 2\omega^2 I_5^{(2)AA} \\
& - A_1^{(1)AA} + \omega^2 A_2^{(1)AA} + (M_B\omega - M_{D^*})^2 A_4^{(1)AA} - 2\omega(M_B\omega - M_{D^*})A_4^{(2)AA} \\
& + \omega^2 A_4^{(3)AA} + 2\omega(M_B\omega - M_{D^*})A_5^{(1)AA} - 2\omega^2 A_5^{(2)AA} \} ,
\end{aligned}$$

Fig. 5 shows these bounds. The perturbative corrections drive the lower bound negative. Again, these lower bounding curves are plotted for reference purposes only. (The lower bound with $\Delta = 2$ GeV is below the range plotted in this graph.)

At $\mathcal{O}(\Lambda_{\text{QCD}}/m_Q)$, the upper bounds will not depend upon λ_1 and λ_2 . However, since $1/(M_{D1} - M_D) \sim 1/\Lambda_{\text{QCD}}$ they will affect the lower bounds. It is possible to obtain the upper bounds to order $\mathcal{O}(\Lambda_{\text{QCD}}^2/m_Q^2)$, since at this order there are no new parameters in the OPE. These corrections only slightly modify the above upper bounds, so we do not show

them here.

VI. COMPARISON WITH MODELS

We choose from the literature the following commonly used form factor models for comparison with our bounds:

- (1) ISGW2 Model [14,15],
- (2) Light-Front Model [16,17],
- (3) BSW II Model [18–20],
- (4) NS Model [21],
- (5) COQM Model [22].

The ISGW2 model is the updated version of the original ISGW model which incorporates the constraints of heavy quark symmetry and relativistic corrections. The BSW II model, derived from the BSW I model by improving the pole structure of form factors, is considered with updated pole masses [23]. The NS model was proposed as a simplified alternative to the NRSX model [24] which specifies the Isgur-Wise function by several strong assumptions such as the pole structure and the condition for the derivative of the single-pole form factor. The form factors are then obtained by employing the heavy quark symmetry relations. The COQM model uses a covariant oscillator quark model to calculate the Isgur-Wise function, and then uses heavy quark symmetry to relate it to the form factors.

Figs. 6–10 are plots for the different form factors from the models and the bounding curves. In plotting these figures, we used $m_b = 4.8$ GeV, $m_c = 1.4$ GeV, $\alpha_s = 0.3$ (corresponding to a scale of about 2 GeV), $\lambda_2 = 0.12$ GeV 2 , $\Delta = 1$ GeV and current PDG data on heavy meson masses. As mentioned above, while λ_2 can be measured from the mass difference $M_{D^*} - M_D$ to a high accuracy, λ_1 and $\bar{\Lambda}$ are not easy to obtain experimentally. Here we pick the parameter set (A) discussed above, $\bar{\Lambda} = 0.4$ GeV, $\lambda_1 = -0.2$ GeV 2 . This uncertainty on λ_1 and $\bar{\Lambda}$ will slightly modify our bounds to the order and kinematic range we are working, as seen from Figs. 1–5.

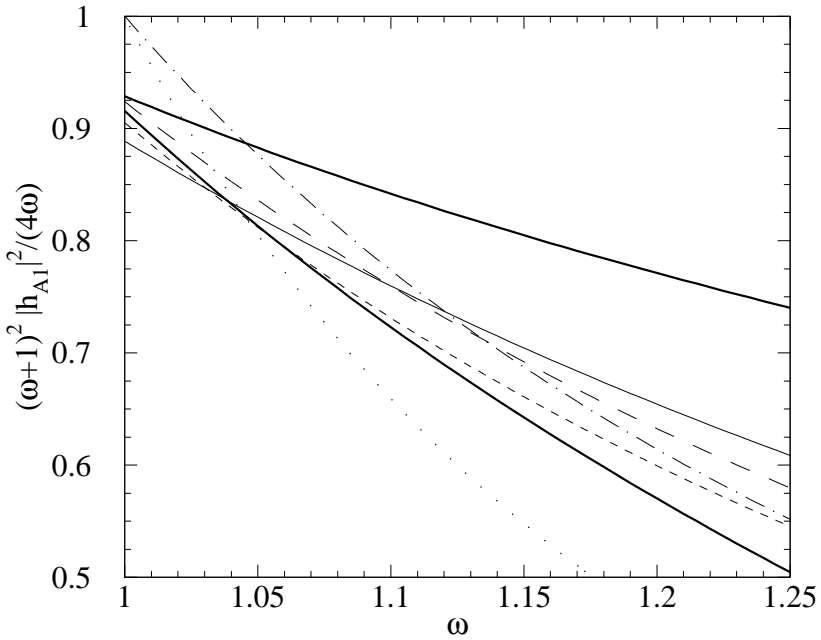


FIG. 6. The model values of $(\omega + 1)^2 |h_{A_1}(\omega)|^2 / (4\omega)$ along with the corresponding bounds for comparison. The thick solid lines are the upper and lower bounds. The thin solid curve is the ISGW2 model. The long dashed curve is the LF model, and the short dashed curve is the BSW II model. The dot-dashed curve is the NS model. The dotted curve is the COQM model.

Fig. 6 shows the model values of $(\omega + 1)^2 |h_{A_1}(\omega)|^2 / (4\omega)$ along with the corresponding bounds for comparison. The first three models have curves falling within or close to the perturbative bounds, while the NS and COQM models have curves slightly off the bounds near zero recoil because they are models designed for the Isgur-Wise function without taking into account the perturbative corrections. The COQM model, however, has a curve which falls far below the lower bound at large ω .

In Fig. 7, the ISGW2 and NS models lie above the upper bound for $(\omega^2 - 1) |\omega h_{A_2} + h_{A_3}|^2 / (4\omega)$ at large recoil, while the other models are closer to our bounds. For $\Delta = 1$ GeV they are above our bounds for most of the kinematic range. If we take $\Delta = 2$ GeV, however, they would be within our bounds. (ISGW2 and NS would still be too large.)

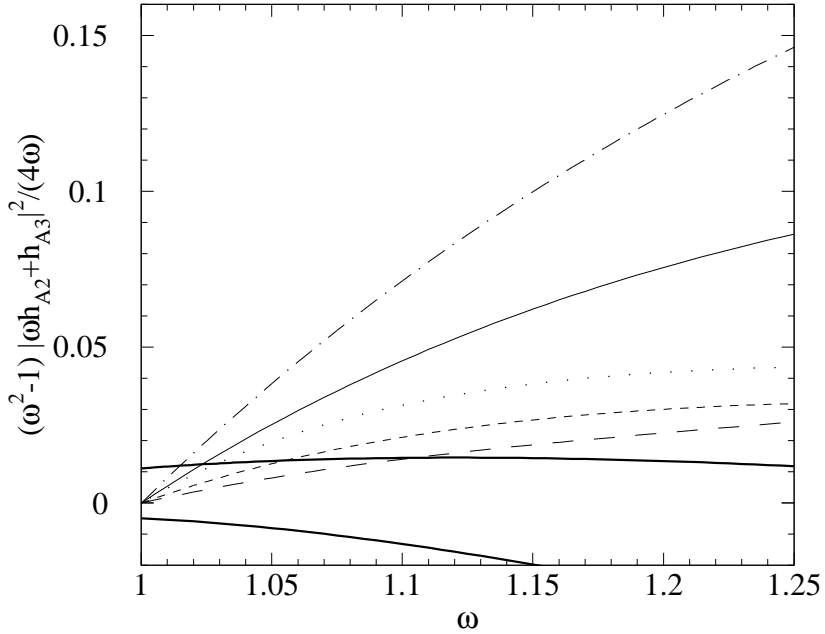


FIG. 7. The model values of $(\omega^2 - 1) |wh_{A2} + h_{A3}|^2 / (4\omega)$ along with the corresponding bounds for comparison. The curves are labeled the same as in Fig. 6.

Only the ISGW2 model predicts a curve near our bounds for $(\omega^2 - 1) |h_V|^2$, shown in Fig. 8; the rest are too small. The Light-Front and BSW II models will be between our bounds when the scale is set at $\Delta = 2$ GeV, but the NS and COQM models still fall below the lower bound.

As shown in Fig. 9, the ISGW2 model agrees with our bounds for $(\omega + 1)^2 |h_+|^2 / \omega$ very well. For the same reason as in Fig. 6, the NS and COQM models start from the position predicted by heavy quark symmetry at zero recoil, without perturbative corrections. The Light-Front, NS, and COQM models stay below the lower bound, and the BSW II model starts above the bounds at $\omega = 1$, then cross the bounds and enter the region under the lower bound. At large recoil, the ISGW2, BSW II, and NS model predictions would lie within the bounds for most of the kinematic range with a larger value for Δ .

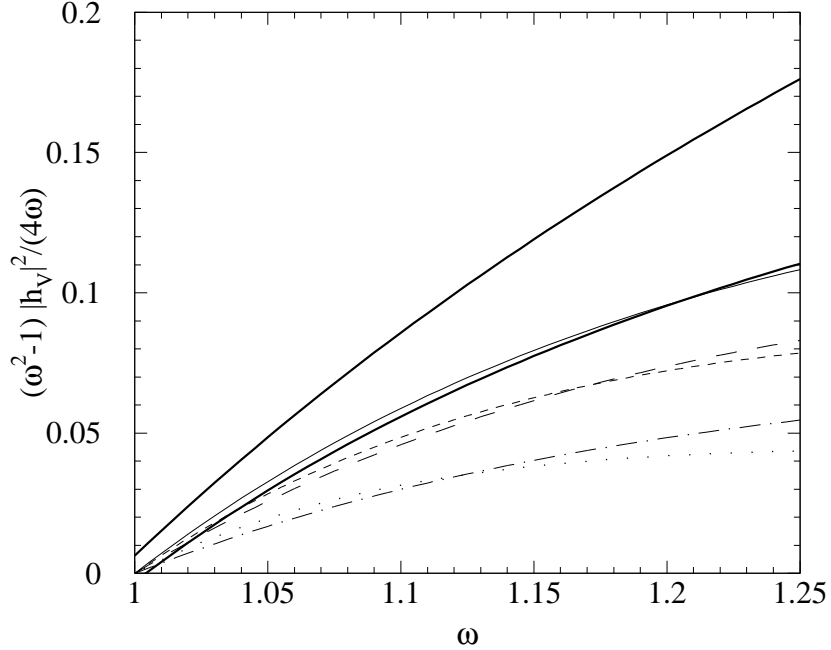


FIG. 8. The model values of $(\omega^2 - 1) |h_V|^2$ along with the corresponding bounds for comparison. The curves are labeled the same as in Fig. 6.

Fig. 10 shows the curves for $(\omega - 1)^2 |h_-|^2 / \omega$, where most models are consistent with our bounds within the kinematic range of interest. The curve for the COQM model is zero, since it uses heavy quark symmetry, which gives $h_-(w) = 0$ in the infinite mass limit.

The scale we choose to plot these diagrams is $\Delta = 1$ GeV, since this gives the tightest bounds. Had we chosen 2 GeV as our working scale, the bounds would be much less stringent and thus would accommodate the models which originally fell slightly outside our bounds in these diagrams.

VII. ORDER $\alpha_s^2 \beta_0$ CORRECTIONS AT ZERO RECOIL

By using the techniques introduced in Ref. [25], we can calculate the $\alpha_s^2 \beta_0$ contribution to the structure functions. Typically, these corrections are about 90% of the full α_s^2 rate, so they can be used as a rough estimate of the next order corrections. The $O(\alpha_s^2 \beta_0)$ correction

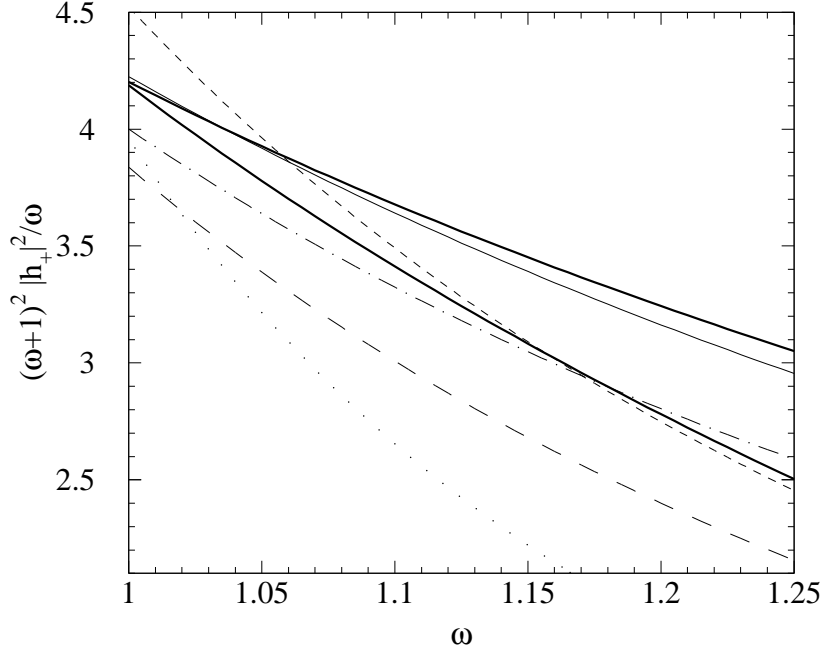


FIG. 9. The model values of $(\omega + 1)^2 |h_+|^2 / \omega$ along with the corresponding bounds for comparison. The curves are labeled the same as in Fig. 6.

to the structure functions, $T_i^{\alpha_s^2 \beta_0}$, can be related to the $O(\alpha_s)$ correction, $T_i^{\alpha_s}(\lambda)$, calculated with a gluon mass λ , as [25]

$$T_i^{\alpha_s^2 \beta_0} = -\beta_0 \frac{\alpha_s^{(V)}(\Delta)}{4\pi} \int_0^\infty \frac{d\lambda^2}{\lambda^2} \left(T_i^{\alpha_s}(\lambda) - \frac{\Delta^2}{\lambda^2 + \Delta^2} T_i^{\alpha_s}(0) \right), \quad (22)$$

where $\alpha_s^{(V)}$ is the strong coupling constant evaluated in the “V-scheme” [26], and is related to the $\overline{\text{MS}}$ coupling constant $\overline{\alpha}_s$ by

$$\alpha_s^{(V)}(\mu) = \overline{\alpha}_s(\mu) + \frac{5}{3} \frac{\overline{\alpha}_s(\mu)^2}{4\pi} \beta_0 + \dots \quad (23)$$

We numerically calculate these corrections at zero recoil. In analogy to Eq. (14), we write the corrections to the moments of the structure as

$$\frac{1}{2\pi i} \int d\epsilon \epsilon^n T_i = I_i^{(n)} + A_i^{(n)}, \quad (24)$$

where $A_i^{(n)}$ now contains both the $O(\alpha_s)$ and the $O(\alpha_s^2 \beta_0)$ contribution to the n^{th} moment of the i^{th} structure function at zero recoil. The results for the $A_i^{(n)}$'s for the zeroth and first

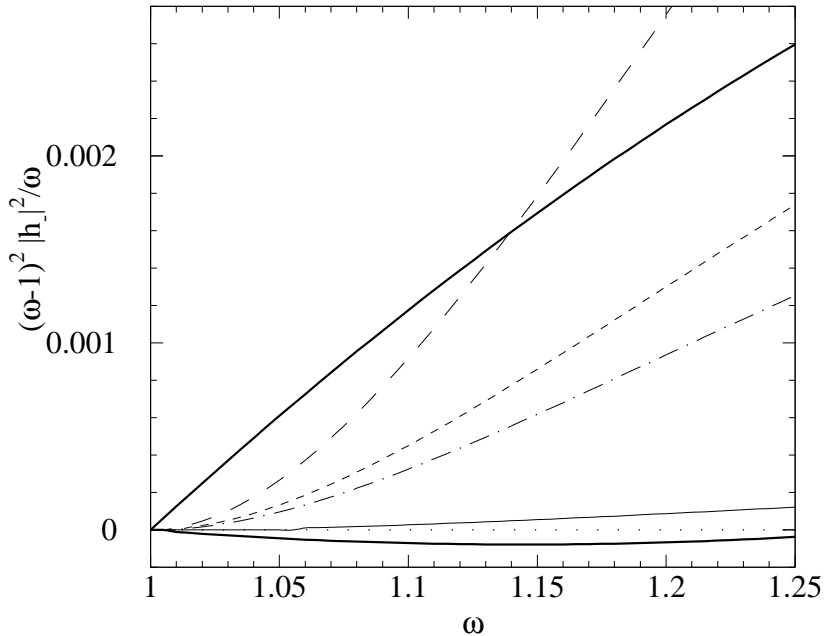


FIG. 10. *The model values of $(\omega - 1)^2 |h_-|^2 / \omega$ along with the corresponding bounds for comparison. The curves are labeled the same as in Fig. 6.*

moments are presented in Table 1, for $\Delta = 1, 2$ GeV. The $O(\alpha_s^2 \beta_0)$ contributions are often large, especially for $\Delta = 1$ GeV. This may be an indication that we need to go to larger Δ to get a reliable perturbative expansion.

If we look at the actual combination of structure functions that appear in our bounds, the situation is more promising. The $O(\alpha_s^2 \beta_0)$ corrections to the upper and lower bounds on the form factors at zero recoil are shown in Table 2 for $\Delta = 1$ GeV. In this case, the $O(\alpha_s^2 \beta_0)$ corrections tend to be rather small, so it seems that the perturbative expansion for the bounds is under control.

VIII. DISCUSSION

As discussed earlier, our bounds on the form factors are derived to order Λ_{QCD}/m_Q and contain leading perturbative QCD corrections. They are constructed to be model indepen-

dent and can be used to test various model predictions for the form factors. Furthermore, they may be used to bound inclusive or exclusive decay rates. The validity of the lower bounds requires the extra assumption of negligible multiparticle production in the decays. This assumption is rather mild, since it is true in the large N_c limit and is supported by current experimental data. The upper bound is rigorously valid without this extra assumption. Therefore, any significant deviation of the phenomenological form factor beyond the upper bound indicates the need for some modification of the model. In general, our bounds are stricter and more accurate near zero recoil.

The bounds become much less stringent when Δ is increased. Therefore, we should use the smallest value of Δ for which there is a reasonable perturbative expansion. We also observed that the $O(\alpha_s^2\beta_0)$ corrections to the bounds at zero recoil are small for $\Delta = 1$ GeV, which in turn suggests that a perturbative expansion in this problem seems to work well, provided that the $O(\alpha_s^2\beta_0)$ corrections dominate in the complete $O(\alpha_s^2)$ corrections.

Among the models we considered in this work, the ISGW2, LF, and BSW II models “pass” most of the qualifications with $\Delta = 2$ GeV. For smaller values of Δ , ISGW2 seems to do the best. However, all models fail, over essentially the whole kinematic range, for the form factor combination $\frac{\omega^2-1}{4\omega} |wh_{A_2} + h_{A_3}|^2$, and thus the models should be modified to satisfy this bound.

ACKNOWLEDGMENTS

The authors would like to thank Fred Gilman and Ira Rothstein for useful discussions. This work was supported in part by the Department of Energy under Grant No. DE-FG02-91ER40682.

APPENDIX: RADIATIVE CORRECTIONS TO THE STRUCTURE FUNCTIONS

The structure functions from perturbative corrections are written in the form $T_i^{JJ} = (\alpha_s/\pi)[U_i^{JJ} + (\omega - 1)V_i^{JJ}]$ for the i th structure function and current J . m_b is the mass of

the b -quark, m_c is the mass of the c -quark, $z \equiv m_c/m_b$, $\omega = v \cdot v'$, and λ is the mass of the gluon used for infrared regularization. We have taken $\lambda \rightarrow 0$ wherever possible.

$$U_1^{VV} = \frac{\epsilon (\epsilon + 2 m_b z) [2 \epsilon^2 + 4 m_b \epsilon z + m_b^2 (3 - 2 z + 3 z^2)]}{9 m_b^2 (\epsilon + m_b z)^3}, \quad (\text{A1})$$

$$\begin{aligned} V_1^{VV} = & - \left[\frac{4}{3} + \frac{1+z}{1-z} \log(z) \right] \delta(\epsilon) \\ & + \frac{z}{45 m_b (\epsilon + m_b z)^5 (\epsilon + 2 m_b z)} [10 \epsilon^6 + 58 m_b \epsilon^5 z - m_b^2 \epsilon^4 (15 + 18 z - 133 z^2) \\ & + m_b^3 \epsilon^3 z (35 - 94 z + 151 z^2) + 2 m_b^4 \epsilon^2 z^2 (135 - 110 z + 47 z^2) \\ & + 8 m_b^5 \epsilon z^3 (45 - 31 z + 5 z^2) + 80 m_b^6 (1 - z) z^4], \end{aligned} \quad (\text{A2})$$

$$\begin{aligned} U_2^{VV} = & - \left[\frac{8}{3 z} + \frac{4 (1+z)}{3 (1-z) z} \log(z) \right] \delta(\epsilon) \\ & - \frac{2}{45 m_b^2 (\epsilon + m_b z)^5} [\epsilon^6 - 3 m_b \epsilon^5 (1 - 2 z) + m_b^2 \epsilon^4 (28 - 13 z + 13 z^2) \\ & - 2 m_b^3 \epsilon^3 (23 - 59 z + 11 z^2 - 6 z^3) - 2 m_b^4 \epsilon^2 z (63 - 96 z + 10 z^2 - 2 z^3) \\ & - 4 m_b^5 \epsilon z^2 (27 - 34 z + 2 z^2) - 40 m_b^6 (1 - z) z^3], \end{aligned} \quad (\text{A3})$$

$$\begin{aligned} V_2^{VV} = & \left[\frac{2 (19 - 62 z + 19 z^2)}{27 (1 - z)^2 z} - \frac{4 (1 - 3 z + 9 z^2 - 3 z^3)}{9 (1 - z)^3 z} \log(z) + \frac{16}{9 z} \log\left(\frac{\lambda}{m_b}\right) \right] \delta(\epsilon) \\ & - \frac{2}{315 m_b z (\epsilon + m_b z)^7 (\epsilon + 2 m_b z)} [7 \epsilon^8 z^2 + \epsilon^7 m_b (280 + 47 z^3) \\ & + \epsilon^6 m_b^2 z (2520 - 196 z - 26 z^2 + 131 z^3) \\ & + \epsilon^5 m_b^3 z^2 (10444 - 1216 z - 186 z^2 + 209 z^3) \\ & + 2 \epsilon^4 m_b^4 z^3 (12060 - 1537 z - 233 z^2 + 109 z^3) \\ & + 2 \epsilon^3 m_b^5 z^4 (15960 - 1905 z - 277 z^2 + 70 z^3) \\ & + 4 \epsilon^2 m_b^6 z^5 (6061 - 550 z - 96 z^2 + 10 z^3) + 8 \epsilon m_b^7 z^6 (1306 - 64 z - 17 z^2) \\ & + 56 m_b^8 z^7 (33 + 2 z)] + \frac{16 \sqrt{\epsilon^2 - \lambda^2}}{9 \epsilon^2 z} + \frac{8 \lambda^2 \sqrt{\epsilon^2 - \lambda^2}}{9 \epsilon^4 z}, \end{aligned} \quad (\text{A4})$$

$$U_4^{VV} = \left[\frac{2}{3 m_b^2 (1 - z) z} + \frac{2}{3 m_b^2 (1 - z)^2 z} \log(z) \right] \delta(\epsilon) \quad (\text{A5})$$

$$+\frac{2 \left[4 \epsilon ^4+m_b \epsilon ^3 \left(11+16 z\right)+m_b^2 \epsilon ^2 z \left(21+26 z\right)+2 m_b^3 \epsilon z^2 \left(9+10 z\right)+20 m_b^4 z^3\right]}{45 m_b^2 \left(\epsilon +m_b z\right)^5},$$

$$\begin{aligned} V_4^{VV} = & -\left[\frac{2 \left(2-z+5 z^2\right)}{9 m_b^2 \left(1-z\right)^3 z}+\frac{2 \left(1-2 z+3 z^2\right)}{3 m_b^2 \left(1-z\right)^4 z} \log (z)\right] \delta (\epsilon) \\ & -\frac{4 z}{315 m_b \left(\epsilon +m_b z\right)^7}\left[14 \epsilon ^5+m_b \epsilon ^4 \left(77+62 z\right)+m_b^2 \epsilon ^3 z \left(125+129 z\right)\right. \\ & \left.+m_b^3 \epsilon ^2 z^2 \left(135+143 z\right)+m_b^4 \epsilon \left(323-28 z\right) z^3+56 m_b^5 z^4\right], \end{aligned} \quad (\text{A6})$$

$$\begin{aligned} U_5^{VV} = & \left[\frac{3-5 z}{3 m_b \left(1-z\right) z}+\frac{1-3 z^2}{3 m_b \left(1-z\right)^2 z} \log (z)\right] \delta (\epsilon) \\ & -\frac{1}{45 m_b^2 \left(\epsilon +m_b z\right)^5}\left[2 \epsilon ^5-2 m_b \epsilon ^4 \left(2-5 z\right)+m_b^2 \epsilon ^3 \left(57-22 z+21 z^2\right)\right. \\ & \left.+m_b^3 \epsilon ^2 z \left(147-46 z+23 z^2\right)+2 m_b^4 \epsilon z^2 \left(63-18 z+5 z^2\right)\right. \\ & \left.+20 m_b^5 \left(3-z\right) z^3\right], \end{aligned} \quad (\text{A7})$$

$$\begin{aligned} V_5^{VV} = & \left[-\frac{13-93 z+69 z^2-25 z^3}{27 m_b \left(1-z\right)^3 z}+\frac{5-14 z+42 z^2-30 z^3+9 z^4}{9 m_b \left(1-z\right)^4 z} \log (z)\right. \\ & \left.-\frac{8}{9 m_b z} \log \left(\frac{\lambda}{m_b}\right)\right] \delta (\epsilon)-\frac{8 \sqrt{\epsilon ^2-\lambda ^2}}{9 \epsilon ^2 m_b z}-\frac{4 \lambda ^2 \sqrt{\epsilon ^2-\lambda ^2}}{9 \epsilon ^4 m_b z} \\ & +\frac{2}{315 m_b z \left(\epsilon +m_b z\right)^7 \left(\epsilon +2 m_b z\right)}\left[140 \epsilon ^7+2 \epsilon ^6 m_b z \left(630-7 z+z^2\right)\right. \\ & \left.+7 \epsilon ^5 m_b^2 z^2 \left(757-16 z+3 z^2\right)+\epsilon ^4 m_b^3 z^3 \left(12339-388 z+85 z^2\right)\right. \\ & \left.+\epsilon ^3 m_b^4 z^4 \left(16345-580 z+131 z^2\right)+\epsilon ^2 m_b^5 z^5 \left(12715-436 z+51 z^2\right)\right. \\ & \left.+2 \epsilon m_b^6 z^6 \left(2963-149 z-7 z^2\right)+28 m_b^7 z^7 \left(37+z\right)\right]. \end{aligned} \quad (\text{A8})$$

$$\begin{aligned} U_1^{AA} = & -\left[\frac{16}{3}+\frac{2 \left(1+z\right)}{1-z} \log (z)\right] \delta (\epsilon) \\ & +\frac{\epsilon \left(\epsilon +2 m_b z\right) \left(2 \epsilon ^2+4 \epsilon m_b z+m_b^2 \left(3+2 z+3 z^2\right)\right)}{9 m_b^2 \left(\epsilon +m_b z\right)^3}, \end{aligned} \quad (\text{A9})$$

$$\begin{aligned} V_1^{AA} = & \left[\frac{4 \left(11-52 z+11 z^2\right)}{27 \left(1-z\right)^2}-\frac{7-3 z+45 z^2-9 z^3}{9 \left(1-z\right)^3} \log (z)+\frac{16}{9} \log \left(\frac{\lambda}{m_b}\right)\right] \delta (\epsilon) \\ & +\frac{1}{45 m_b \left(\epsilon +m_b z\right)^5}\left[10 \epsilon ^5 z-2 \epsilon ^4 m_b \left(40-19 z^2\right)-\epsilon ^3 m_b^2 z \left(415+38 z-57 z^2\right)\right] \end{aligned}$$

$$\begin{aligned}
& -\epsilon^2 m_b^3 z^2 (735 + 110 z - 37 z^2) - 4 \epsilon m_b^4 z^3 (125 + 22 z - 5 z^2) \\
& - 40 m_b^5 z^4 (4 + z) \Big] + \frac{16 \sqrt{\epsilon^2 - \lambda^2}}{9 \epsilon^2} + \frac{8 \lambda^2 \sqrt{\epsilon^2 - \lambda^2}}{9 \epsilon^4}, \tag{A10}
\end{aligned}$$

$$\begin{aligned}
U_2^{AA} = & - \left[\frac{4}{z} + \frac{4 (1 + z)}{3 z (1 - z)} \log(z) \right] \delta(\epsilon) \\
& - \frac{2}{45 m_b^2 (\epsilon + m_b z)^5} \left[\epsilon^6 - 3 \epsilon^5 m_b (1 - 2 z) + \epsilon^4 m_b^2 (28 - 17 z + 13 z^2) \right. \\
& \left. - 2 \epsilon^3 m_b^3 (23 - 53 z + 19 z^2 - 6 z^3) - 2 \epsilon^2 m_b^4 z (75 - 78 z + 20 z^2 - 2 z^3) \right. \\
& \left. - 4 \epsilon m_b^5 z^2 (39 - 28 z + 4 z^2) - 40 m_b^6 (1 - z) z^3 \right], \tag{A11}
\end{aligned}$$

$$\begin{aligned}
V_2^{AA} = & \left[\frac{2 (43 - 110 z + 43 z^2)}{27 (1 - z)^2 z} - \frac{4 (1 - 3 z - 9 z^2 + 3 z^3)}{9 (1 - z)^3 z} \log(z) + \frac{16}{9 z} \log\left(\frac{\lambda}{m_b}\right) \right] \delta(\epsilon) \\
& - \frac{2}{315 m_b z (\epsilon + m_b z)^7 (\epsilon + 2 m_b z)} \left[7 \epsilon^8 z^2 + \epsilon^7 m_b (280 + 47 z^3) \right. \\
& \left. + \epsilon^6 m_b^2 z (2520 - 196 z + 2 z^2 + 131 z^3) \right. \\
& \left. + \epsilon^5 m_b^3 z^2 (10444 - 1048 z + 18 z^2 + 209 z^3) \right. \\
& \left. + 2 \epsilon^4 m_b^4 z^3 (12312 - 1069 z + 29 z^2 + 109 z^3) \right. \\
& \left. + 2 \epsilon^3 m_b^5 z^4 (17028 - 1077 z + 13 z^2 + 70 z^3) \right. \\
& \left. + 4 \epsilon^2 m_b^6 z^5 (6601 - 316 z - 30 z^2 + 10 z^3) + 8 \epsilon m_b^7 z^6 (1282 - 58 z - 13 z^2) \right. \\
& \left. + 56 m_b^8 z^7 (33 + 2 z) \right] + \frac{16 \sqrt{\epsilon^2 - \lambda^2}}{9 \epsilon^2 z} + \frac{8 \lambda^2 \sqrt{\epsilon^2 - \lambda^2}}{9 \epsilon^4 z}, \tag{A12}
\end{aligned}$$

$$\begin{aligned}
U_4^{AA} = & - \left[\frac{2 (1 + 3 z)}{3 m_b^2 z (1 - z)^2} - \frac{2 (1 - 5 z)}{3 m_b^2 z (1 - z)^3} \log(z) \right] \delta(\epsilon) \tag{A13} \\
& + \frac{2 [4 \epsilon^4 + \epsilon^3 m_b (11 + 16 z) + \epsilon^2 m_b^2 z (45 + 26 z) + 2 \epsilon m_b^3 z^2 (33 + 10 z) + 20 m_b^4 z^3]}{45 m_b^2 (\epsilon + m_b z)^5},
\end{aligned}$$

$$\begin{aligned}
V_4^{AA} = & \left[\frac{2 (6 - 19 z - 46 z^2 + 11 z^3)}{9 m_b^2 z (1 - z)^4} - \frac{2 (1 - 7 z + 25 z^2 - 3 z^3)}{3 m_b^2 z (1 - z)^5} \log(z) \right] \delta(\epsilon) \\
& - \frac{4 z}{315 m_b (\epsilon + m_b z)^7} \left[14 \epsilon^5 + \epsilon^4 m_b (77 + 62 z) + \epsilon^3 m_b^2 z (377 + 129 z) \right. \\
& \left. + \epsilon^2 m_b^3 z^2 (699 + 143 z) + \epsilon m_b^4 (275 - 28 z) z^3 + 56 m_b^5 z^4 \right], \tag{A14}
\end{aligned}$$

$$\begin{aligned}
U_5^{AA} = & \left[\frac{7 - 5 z}{3 m_b (1 - z) z} + \frac{(1 + 4 z - 3 z^2)}{3 m_b (1 - z)^2 z} \log(z) \right] \delta(\epsilon) \\
& + \frac{1}{45 m_b^2 (\epsilon + m_b z)^5} \left[-2 \epsilon^5 + 2 \epsilon^4 m_b (2 - 5 z) - \epsilon^3 m_b^2 (57 - 10 z + 21 z^2) \right. \\
& \quad \left. - \epsilon^2 m_b^3 z (195 - 10 z + 23 z^2) - 2 \epsilon m_b^4 z^2 (111 - 6 z + 5 z^2) \right. \\
& \quad \left. - 20 m_b^5 (3 - z) z^3 \right], \tag{A15}
\end{aligned}$$

$$\begin{aligned}
V_5^{AA} = & - \left[\frac{(61 - 225 z + 81 z^2 - 25 z^3)}{27 m_b (1 - z)^3 z} - \frac{(5 - 26 z + 90 z^2 - 42 z^3 + 9 z^4)}{9 m_b (1 - z)^4 z} \log(z) \right. \\
& \quad \left. + \frac{8}{9 m_b z} \log\left(\frac{\lambda}{m_b}\right)\right] \delta(\epsilon) - \frac{8 \sqrt{\epsilon^2 - \lambda^2}}{9 \epsilon^2 m_b z} - \frac{4 \lambda^2 \sqrt{\epsilon^2 - \lambda^2}}{9 \epsilon^4 m_b z} \\
& + \frac{2}{315 m_b z (\epsilon + m_b z)^7 (\epsilon + 2 m_b z)} \left[140 \epsilon^7 + 2 \epsilon^6 m_b z (630 - 7 z + z^2) \right. \\
& \quad \left. + 7 \epsilon^5 m_b^2 z^2 (757 - 4 z + 3 z^2) + \epsilon^4 m_b^3 z^3 (12843 + 80 z + 85 z^2) \right. \\
& \quad \left. + \epsilon^3 m_b^4 z^4 (18481 + 248 z + 131 z^2) + \epsilon^2 m_b^5 z^5 (14875 + 32 z + 51 z^2) \right. \\
& \quad \left. + 2 \epsilon m_b^6 z^6 (2867 - 137 z - 7 z^2) + 28 m_b^7 z^7 (37 + z) \right]. \tag{A16}
\end{aligned}$$

REFERENCES

- [1] N. Isgur and M.B. Wise, Phys. Lett. **B232**, 113 (1989).
- [2] N. Isgur and M.B. Wise, Phys. Lett. **B237**, 113 (1990).
- [3] A.F. Falk, H. Georgi, B. Grinstein, and M.B. Wise, Nucl. Phys. **B343**, 1 (1990).
- [4] C.G. Boyd, B. Grinstein, R.F. Lebed, Nucl. Phys **B461**, 493 (1996); Phys. Rev. **D56** 6895 (1997); I. Caprini, L. Lellouch, M. Neubert, Nucl. Phys. **B530**, 153 (1998).
- [5] I. Bigi, M. Shifman, N.G. Uraltsev, and A. Vainshtein, Phys. Rev. **D52**, 196-235 (1995).
- [6] C.G. Boyd and I.Z. Rothstein, Phys. Lett. **B395**, 96 (1997).
- [7] C.G. Boyd and I.Z. Rothstein, Phys. Lett. **B420**, 350 (1998).
- [8] C.G. Boyd, Z. Ligeti, I.Z. Rothstein, and M.B. Wise, Phys. Rev. **D55**, 3027-3037 (1997).
- [9] B. Blok, L. Koyrakh, M. Shifman, and A. I. Vainshtein, Phys. Rev. **D49**, 3356 (1994).
- [10] C.G. Boyd, B. Grinstein, and A.V. Manohar, Phys. Rev. **D54**, 2081-2096 (1996).
- [11] A.V. Manohar and M.B. Wise, Phys. Rev. **D49**, 1310 (1994).
- [12] A. Kapustin, Z. Ligeti, M.B. Wise, and B. Grinstein, Phys. Lett. **B375**, 327-334 (1996).
- [13] M. Gremm, A. Kapustin, Z. Ligeti, and M.B. Wise, Phys. Rev. Lett. **77**, 20 (1996).
- [14] N. Isgur, D. Scora, B. Grinstein, and M.B. Wise, Phys. Rev. **D39**, 799-818 (1989).
- [15] D. Scora and N. Isgur, Phys. Rev. **D52**, 2783-2812 (1995).
- [16] W. Jaus, Phys. Rev. **D41**, 3394 (1990); **44**, 2851 (1991).
- [17] H-Y. Cheng, C-Y. Cheung, and C-W. Hwang, Phys. Rev. **D55**, 1559-1577 (1997).
- [18] M. Wirbel, B. Stech, and M. Bauer, Z. Phys. **C29**, 637 (1985).
- [19] M. Bauer, B. Stech, and M. Wirbel, Z. Phys. **C34**, 103 (1987).
- [20] J.G. Korner and G.A. Schuler, Z. Phys. **C38**, 511 (1988), Erratum-ibid. **C41**, 690 (1989).
- [21] M. Neubert and B. Stech, in: Heavy Flavours, Second Edition, edited A.J. Buras and M. Lindner (World Scientific, Singapore, 1998), p294-344.
- [22] R. Mohanta, A.K. Giri, M.P. Khana, M. Ishida, S. Ishida, and M. Oda, Prog. Theor. Phys. **4**, 101 (1999).
- [23] A. Abd El-Hady, M.A.K. Lodhi, and J.P. Vary, Phys. Rev. **D59**, 094001 (1999).
- [24] M. Neubert, V. Rieckert, B. Stech, and Q.P. Xu, in: Heavy Flavours, First Edition, edited by A.J. Buras and M. Lindner (World Scientific, Singapore, 1992), p 286.
- [25] B.H. Smith and M.B. Voloshin, Phys. Lett. **B340**, 176 (1994).
- [26] S.J. Brodsky, G.P. Lepage, and P.B. MacKenzie, Phys. Rev. **D28** 228 (1983).

	$\Delta = 1 \text{ GeV}$		$\Delta = 2 \text{ GeV}$	
	$O(\alpha_s)$	$O(\alpha_s^2 \beta_0)$	$O(\alpha_s)$	$O(\alpha_s^2 \beta_0)$
$A_1^{(0)AA}$	-0.071	0.016	-0.059	0.005
$A_1^{(1)AA}$	0.0053	0.0040	0.024	0.018
$A_2^{(0)AA}$	-0.13	0.21	-0.042	0.22
$A_2^{(1)AA}$	0.086	0.057	0.21	0.15
$A_4^{(0)AA}$	-0.015	0.003	-0.013	-0.0004
$A_4^{(1)AA}$	0.0023	0.0014	0.0054	0.0036
$A_5^{(0)AA}$	0.032	-0.033	0.015	-0.034
$A_5^{(1)AA}$	-0.017	-0.011	-0.041	-0.029
$A_1^{(0)VV}$	0.0063	0.0042	0.015	0.011
$A_1^{(1)VV}$	0.0038	0.0022	0.017	0.011
$A_2^{(0)VV}$	0.26	0.13	0.32	0.24
$A_2^{(1)VV}$	0.062	0.042	0.14	0.10
$A_4^{(0)VV}$	-0.0060	0.0012	-0.0048	0.0002
$A_4^{(1)VV}$	0.0014	0.0009	0.0032	0.0022
$A_5^{(0)VV}$	-0.022	-0.024	-0.034	-0.037
$A_5^{(1)VV}$	-0.012	-0.008	-0.029	-0.021

TABLE I. Order α_s and $\alpha_s^2 \beta_0$ corrections to the moments of the structure functions at zero recoil, evaluated for $\Delta = 1, 2 \text{ GeV}$. For this table, $\alpha_s = 0.3$, and $n_f = 4$.

	Tree Level	$O(\alpha_s)$	$O(\alpha_s^2 \beta_0)$
Upper $\frac{(\omega+1)^2}{4\omega} h_{A_1} ^2$	1	-0.071	0.016
Lower $\frac{(\omega+1)^2}{4\omega} h_{A_1} ^2$	1	-0.084	0.006
Upper $\frac{\omega^2-1}{4\omega} \omega h_{A_2} + h_{A_3} ^2$	0	0.011	0.007
Lower $\frac{\omega^2-1}{4\omega} \omega h_{A_2} + h_{A_3} ^2$	0	-0.005	-0.001
Upper $\frac{\omega^2-1}{4\omega} h_V ^2$	0	0.006	0.004
Lower $\frac{\omega^2-1}{4\omega} h_V ^2$	0	-0.003	-0.001
Upper $\frac{(\omega+1)^2}{\omega} h_+ ^2$	4	0.20	-0.05
Lower $\frac{(\omega+1)^2}{\omega} h_+ ^2$	4	0.19	-0.06
Upper $\frac{(\omega-1)^2}{\omega} h_- ^2$	0	0	0
Lower $\frac{(\omega-1)^2}{\omega} h_- ^2$	0	0	0

TABLE II. Bound on form factors at zero recoil, evaluated with $\Delta = 1$ GeV.